physica status solidi a
www.pss-a.com

Check for updates

Next-Generation Application-Based Artificial Intelligence in Modeling and Estimation for Ni/n-GaAs/In Schottky Barrier Diode

*Hülya Doğan and Serdar Kockanat**

Herein, for Ni/n-GaAs/In Schottky barrier diode, experimental measurement, modeling, data generation from the model, and parameter estimation processes are simultaneously carried out. In the experimental step, Ni/n-GaAs/In Schottky barrier diodes are fabricated and annealed from the temperature of 200 °C up to 600 °C with 100 °C steps. Current values are recorded by applying voltage to the diode contacts from −1 V up to 0.5 V. In the modeling step, 1503 experimental current–voltage data are used for 19 different regression models. For Adaptive Neuro Fuzzy System (ANFIS), when root mean square error, mean square error, mean absolute error, and coefficient of determination are calculated 6.0341e-07, 3.6410e-13, 2.3873e-07, and 0.9999 for training, they are obtained 5.8904e-07, 3.4697e-13, 2.3083e-07, and 0.9999 for testing. In the estimation step, the values of electrical parameters are estimated by using Mayfly algorithm. Estimations are performed for all annealing temperatures. In addition, current–voltage data for the annealing temperature of 350 °C are produced by the ANFIS model. Thus, a new-generation artificial intelligence application, that includes measurement, modeling, and estimation for the Ni/n-GaAs/In Schottky barrier diode with varying annealing temperatures, is realized and a new perspective is provided to researchers and practitioners.

1. Introduction

Schottky barrier diode (SBD) is called metal–semiconductor diode and it has an important role in the area of electronic circuit elements industry and technology. SBDs are frequently used in many fields such as switching circuits, solar cells, semiconductor detector applications, microwave circuit elements, and modulators.[1–3] The quality of the interface depends on between deposited Schottky metal and semiconductor surface and it plays an important role in the electrical performance of the SBD. Surface defects and native oxide at the metal/GaAs interface can cause problems with the traditional method of manufacturing connections, which involves the deposition of metallic coatings on GaAs.[4–9] Thermal annealing behavior of SBDs is of great interest for both scientific and technological reasons.[4,5] Due to thermal annealing, thermodynamics can be used to explain interdiffusion, contaminations, chemical reactions, compound formation, interface roughening, defect generation, dopant migration, a flat diode interface, etc.[8–10] The performances of SBDs are largely determined by the quality of the interface between the deposited Schottky metal and the semiconductor surface.[9] The most preferred method to improve the stability and performance of metal semiconductor diodes is the thermal annealing of the metal–semiconductor structure after the necessary metal contacts are formed on the surfaces of the semiconductor substrate. With this method, the Schottky barrier height can be improved by means of reactive or refractory (resistant to high-temperature annealing) metals evaporated as Schottky contact (rectifying contact) to the semiconductor surface. Also, the reactive metal reduces the native oxide layer and reacts with the semiconductor substrate during annealing even for metal deposition at room temperature.[6–8] A reacted contact has a substantially higher quality than an unannealed sample and is thermodynamically stable.[7,8]

Today, progress in computer technologies has triggered the development of artificial intelligence. Therefore, artificial intelligence has attracted the attention of many researchers in the fields of physics, engineering, and health. Also, it is effectively used in the solution of many scientific problems.[11–16] Artificial intelligence is known the transfer of human abilities to computers with the aid of machine learning. At this point, machine learning plays an important role. Classification, clustering, and regression are popular machine learning techniques. Especially, the regression methods analyze the modeling of one or more input predictors for an output response. Thus, it is possible to model many systems using input and output data and to predict possible output values for new inputs through these designed models. In recent years, regression trees, linear regression (LR), support vector machines (SVM), and Gaussian process regression

H. Doğan, S. Kockanat
Department of Electrical and Electronics Engineering
Engineering Faculty
Sivas Cumhuriyet University
Sivas 58140, Turkey
E-mail: skockanat@cumhuriyet.edu.tr

S. Kockanat
Applied Optimization and DSP Research Lab.
Department of Electrical and Electronics Engineering
Sivas Cumhuriyet University
Sivas 58140, Turkey

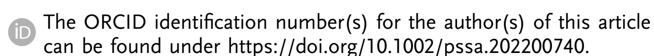
The ORCID identification number(s) for the author(s) of this article can be found under https://doi.org/10.1002/pssa.202200740.

DOI: 10.1002/pssa.202200740

 © 2023 Wiley-VCH GmbH

(GPR) techniques are effectively used in system modeling for regression.[17–19]

In the literature, many different machine learning methods have been successfully realized in the modeling of current–voltage (I–V) characterization of the SBDs. This topic has attracted the attention of researchers and SBD models have been created for different measurement temperatures and semiconductor materials. Torun and Dogan produced Au/Ni/n-GaN/undoped GaN SBD and measured current and voltage values of SBD between 40 K and 400 K temperatures. In addition, voltage measurements were made between -2 and $+2$ V. Thus, 5192 data were obtained for I–V characteristics in total. Using measured data, a system is modeled to estimate current values using Adaptive Neuro Fuzzy System (ANFIS). In this model, when the voltage and temperature are inputs, the current is output. The performance of the proposed model was compared with those of the other machine learning methods such as SVM and GPR for training and test phases. For training and test phases, root mean square (RMSE) error results of proposed model are 6.231e-06 and 6.806e-06, respectively.[20]

Güzel et al. designed a model of 6H–SiC/MEH-PPV SBD. Similarly, when the temperature and voltage data are input, the current data are output. In this model, artificial neural network (ANN) is used for model design and the measured current data were collected between 100 and 250 K temperatures. Also, the voltage measurement is realized between -3 and $+3$ V. For suggested ANN model, mean square error (MSE) and coefficient of determination (R) values are obtained 1.63e-08 and 0.99999, respectively.[21] Çolak et al. performed temperature measurements between 100 and 300 K and voltage measurements between -2 V and $+3$ V for the SBD model. They created a model using ANN with feed-forward back-propagation using 362 measured experimental data. Thus, they tried to estimate the I–V characteristic of the SBD. For proposed ANN model, MSE and R values are obtained 7.65906e-07 and 0.99992, respectively.[22]

Recently, while the characterization modeling of the SBDs with machine learning techniques are realized in the literature, the electrical parameter estimation of SBD come to the fore. Various artificial intelligence methods, such as optimization and neural networks, have been used for parameter estimation of SBD. Güzel and Çolak proposed a machine learning method to estimate the characteristic parameters of SBD. An ANN model was developed using 368 experimental data. The margins of error for the ideality factor (n) and the series resistance (R_s) were found to be 1.645 and 5.694, respectively.[23] Olikh studied the parameter estimation of SBD using I–V characteristics. Barrier height (ϕ_b), n, and R_s parameters were estimated using ten analytical methods, four optimization algorithms, and two analytical methods. The advantages and disadvantages of the proposed methods are presented.[24] Chang et al. investigated the parameter estimation of SBD by genetic algorithm (GA) using experimental data. The proposed approach gave better results than those of the Cheung method.[25] Karaboga et al. proposed an approach-based modified artificial bee colony (ABC) algorithm for parameter estimation. Estimation performance of ABC algorithm was compared with those of the particle swarm optimization (PSO) and differential evolution (DE). Proposed approach gives satisfactory results.[26] Güzel and Çolak suggested an ANN method with capacitance–voltage (C–V) data for 6H-SiC/MEH-PPV/Al SBD. In total, 480 experimental data were employed. For the proposed approach, MSE and R values are calculated 4.34e-06 and 0.99728, respectively.[27] Rabehi et al. proposed an approach-based equilibrium optimizer algorithm for parameter extraction of SBD. The performance of the employed optimization algorithm was compared with those of the Cheung and Kaminski methods. For the suggested approach, ϕ_b, R_s, and n are calculated 0.62 eV, 16.21 Ω, and 1.88, respectively.[28]

In this study, Ni/n-GaAs SBD contacts were fabricated and annealed from the annealing temperature of 200 °C up to 600 °C with 100 °C steps. In the thermal annealing process, the furnace was heated to the desired annealing temperature. Then, the SBD contacts were annealed for a certain time in the furnace. After cooling, the SBD contacts were ready for measurement and I–V measurements were realized at room temperature. Here, the aim of annealing is to make the annealed Schottky contacts more stable than the unannealed Schottky contacts in the point of thermodynamics.[9] It should be noted that I–V measurement at changing room temperature with the aid of helium cryostat is not the same as I–V measurement at changing annealing temperature. For each annealing temperature, voltage measurement was carried out from -1 V up to $+0.5$ V with 0.005 V steps and the current values corresponding to the voltage values were recorded. Thus, in total, 1503 data were obtained. In order to model I–V characteristic of Ni/n-GaAs SBD for annealing process, five different regression analysis methods and their subgroups, which are frequently used in the literature, were used together with ANFIS because, in the literature, these aforementioned methods can give successful results for the modeling of semiconductor processes with nonlinear and uncertain characteristics such as thermal annealing. Finally, the thermal annealing process was modeled using 19 different regression analysis methods with 1503 measured data. Then, all models are compared for different error performances. Thus, using the successful model of SBD, I–V dataset can be produced for the desired annealing temperature without costly and time-consuming experiments. One of the most innovative aspects of this work is that the I–V modeling of Ni/n-GaAs SBD is first analyzed for the thermal annealing process because, herein, I–V measurements were made for five different annealing temperatures. This situation is not included for any study in the literature. For example, Dogan et al. proposed an ANN method for I–V characteristic model of annealed and unannealed Ni/n-type 6H–SiC SBD. In that model, the I–V measurements were realized between temperature of 80 and 500 K. However, only 900 °C is determined for thermal annealing of Ni/n-type 6H–SiC SBD. As a result, the analysis of the thermal annealing process, which cannot be expressed with any mathematical formula such as thermionic emission equation, was carried out in this study.[7–9]

After modeling the I–V characteristic of SBD for thermal annealing, unlike other studies in the literature, I–V data were generated for the annealing temperature of 350 °C, which was not used in the training and testing stages. And, its accuracy was demonstrated. Thus, the desired I–V data of SBD were achieved without additional experiment and the abovementioned objectives were realized for modeling using regression methods.

In addition, for annealing temperatures of 200, 300, 400, 500, 600, and 350 °C, electrical parameters of SBD were quickly

© 2023 Wiley-VCH GmbH

18626319, 2023, 6, Downloaded from https://onlinelibrary.wiley.com/doi/10.1002/pssa.202200740 by Cumhuriyet University, Wiley Online Library on [10/01/2024]. See the Terms and Conditions (https://onlinelibrary.wiley.com/terms-and-conditions) on Wiley Online Library for rules of use; OA articles are governed by the applicable Creative Commons License

physica status solidi a
www.pss-a.com

estimated from I–V characteristics with high precision by artificial intelligence algorithm. For electrical characterization of SBD, Mayfly algorithm (MA) was first used in the literature for the estimation of the n, ϕ_b, and R_s values because this algorithm gave more successful results in solar cell parameter estimation than those of other used optimization algorithms.[29] In addition, recently, the MA has been used successfully in solving many current scientific problems.[30–33] Especially, in the electrical parameter estimation of SBD, an artificial intelligence approach was applied instead of classical methods, such as Ln I–V, Norde, and Cheung. So, for the whole I–V data of forward biasing, electrical parameter estimation was performed without additional functions or methods.

To the best of our knowledge, there is no article in the literature that includes experimental fabrication and measurement, modeling I–V characteristic, data generation, and electrical parameter estimation of Ni/n-GaAs/In SBD for varying thermal annealing temperature. In addition, all these stages were practically carried out with new-generation method-based artificial intelligence algorithms. **Figure 1** shows the flow chart of three-stage application.

2. Experimental Section

2.1. Experimental Details

In this article, silicon-doped n-type GaAs with a (100) oriented free carrier density of 7.3×10^{15} cm^{-3} was used.[9] For 5 min, the wafer was successively degreased in trichloroethylene, acetone, and methanol. For 1 min, H_2SO_4:H_2O_2:H_2O (5:1:1) was used to etch the degreased wafer for removing any surface damage and unwanted contaminants. The metal was evaporated to the matte side of the cleaned GaAs surface using the thermal evaporation method. Then, in order to further reduce the resistance of the ohmic contact, the backside ohmic contact was formed by annealing in N_2 environment at 300 °C for 3 min. Schottky contacts were formed as dots with a diameter of about 1.5 mm on the faceplate of the parts using Ni evaporation. The Schottky contacts were created on the front face of the parts as dots with a diameter of approximately 1.5 mm using Ni evaporation. The vacuum coating unit was used for all evaporation processes at a pressure of roughly 10^{-5} mbar. In an environment of N_2, a quartz tube furnace was used to conduct the thermal annealing. After SBD production, the diodes were annealed in a N_2 environment from annealing temperature of 200–600 °C with 100 °C steps for 1 min. Keithley's 487 Picoammeter/Voltage source was used to measure the I–V characteristics of SBDs in the dark at room temperature.

2.2. Modeling of I–V Characteristic of Ni/n-GaAs/In SBD

In this study, as explained in the previous section, 1503 I–V data were obtained from the thermal annealing process. When 80% of this data were randomly allocated for the training phase, 20% of this data were selected for the testing phase.[34] So, 1203 and 300 data were selected for training and testing, respectively. In addition, annealing temperature and voltage were configured as inputs and current was determined as output in model creation.

ANFIS, LR, trees regression (TR), SVM, ensemble tree, and GPR methods were used to model the Ni/n-GaAs/In SBD for thermal annealing. LR has four subgroups: linear, interactions, robust, and stepwise. LR is a well-known method used for linear and continuous variables. TR has three subgroups as fine, medium, and coarse. TR is a decision tree included in regression methods and it can be used to predict continuous value outputs. Linear, fine, medium, and coarse Gaussian kernels are four

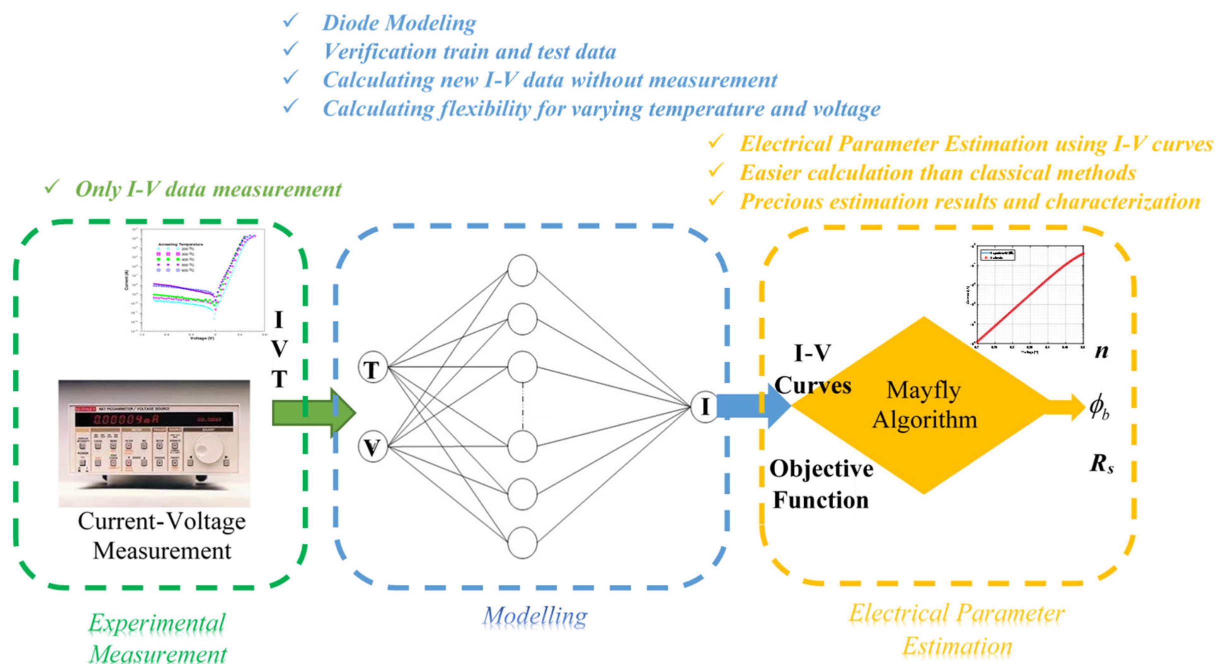

Figure 1. Flow chart of three-stage application and highlights of this study.

© 2023 Wiley-VCH GmbH
18626319, 2023, 6, Downloaded from https://onlinelibrary.wiley.com/doi/10.1002/pssa.202200740 by Cumhuriyet University, Wiley Online Library on [10/01/2024]. See the Terms and Conditions (https://onlinelibrary.wiley.com/terms-and-conditions) on Wiley Online Library for rules of use; OA articles are governed by the applicable Creative Commons License

18626319, 2023, 6, Downloaded from https://onlinelibrary.wiley.com/doi/10.1002/pssa.202200740 by Cumhuriyet University, Wiley Online Library on [10/01/2024]. See the Terms and Conditions (https://onlinelibrary.wiley.com/terms-and-conditions) on Wiley Online Library for rules of use; OA articles are governed by the applicable Creative Commons License

subgroups of SVM.[35] SVM is a machine learning method that finds a decision boundary between the two classes that are furthest from any point in the training data.[36] GPR has five subgroups including rational quadratic, squared exponential, matern 5/2, matern 3/2, and exponential kernels.[37] It is a nonparametric regression model that can predict unknown output value using the Gaussian Process. Ensemble of regression tree and bootstrap-aggregated of regression tree models are the other two types of efficient tree models. In the literature, the abovementioned methods have been successfully used for SBD modeling and comparative performance evaluation was made.[20] However, in this study, the all values of MAE, MSE, RMSE, and R functions applied by aforementioned methods are also demonstrated as a plus feature.

The aforementioned 19 regression methods were realized to model I–V characteristic of Ni/n-GaAs/In SBD for thermal annealing process using 1203 training and 300 test data. Then, for both training and test stages, the performances of competitor methods were compared using error functions such as mean absolute error (MAE), MSE, and RMSE.[20–22] MAE, MSE, and RMSE functions give current values and their units are ampere (A).

$$\text{MAE} = \frac{1}{n}\sum_{i=1}^{n} |I_{\text{e}_i} - I_{\text{est}_i}| \tag{1}$$

$$\text{MSE} = \frac{1}{n}\sum_{i=1}^{n} (I_{\text{e}_i} - I_{\text{est}_i})^2 \tag{2}$$

$$\text{RMSE} = \sqrt{\text{MSE}} = \sqrt{\frac{1}{n}\sum_{i=1}^{n} (I_{\text{e}_i} - I_{\text{est}_i})^2} \tag{3}$$

where n is the data sample number, I_e is the experimental current, and I_est is the estimated current by regression models. Also, the other performance indicator is R and it is given as[23]

$$R = \sqrt{1 - \frac{\sum_{i=1}^{n} (I_{\text{e}_i} - I_{\text{est}_i})^2}{\sum_{i=1}^{n} (I_{\text{e}_i})^2}} \tag{4}$$

The MAE error is the average of the absolute values of the difference between the actual and predicted values. It is used in regression analyzes where negative errors are considered. In MSE, the mean of the squares of the difference values is calculated. So, from the perspective of mathematics, high estimation errors become more visible than small estimation errors. RMSE is the square root of MSE and it shows better error performance than MSE. RMSE not only preserves the mathematical visibility of estimation errors, but also helps to calculate the error in its true unit. For the aforementioned reasons, to analyze the error performance of proposed studies, the calculation of MAE, MSE, RMSE, and R values are frequently used by many researchers.[15,20,23,27,29]

2.2.1. Declaration of ANFIS

In recent years, ANFIS has emerged as a method used in regression analysis. It is proposed by Jang in 1993 and employed for nonlinear modeling using the fuzzy logic and ANN.[38] ANFIS contains an adaptive inference model that is consisted in Mamdani or Takagi–Sugeno inference model.[39] The complete system occurs in five stages. These stages are fuzzification, product, normalized, defuzzification, and output, respectively.

In this study, for the modeling of Ni/n-GaAs/In SBD, ANFIS is realized and it uses an algorithm to recognize parameters of Sugeno-type fuzzy inference system. For ANFIS, X and Y inputs are voltage (V) and annealing temperature (T) and f output is the current of Ni/n-GaAs/In SBD. Type of Sugeno fuzzy inference systems has m fuzzy rules; type of Sugeno fuzzy inference systems has two fuzzy rules:

Rule 1: If (voltage is A1) and (annealing temperature is B1), then $f_1 = p_1 V + q_1 T + r_1$

Rule m: If (voltage is A2) and (annealing temperature is B2), then $f_2 = p_2 V + q_2 T + r_2$

In this rules, while A1, A2 and B1, B2 are nonlinear parameters, other parameters are linear. ANFIS architecture is shown in **Figure 2**. In stage 1, voltage and current are the input of nodes A1, B1 and A2, B2, respectively. A1, A2, B1, and B2 are the linguistic labels used in the fuzzy theory for dividing the membership functions. The membership relationship can be expressed as follows

$$\begin{aligned} O_{1,i} &= \mu_{\text{A}_i}(x), i = 1, 2 \\ O_{1,j} &= \mu_{\text{B}_j}(y), i = 1, 2 \end{aligned} \tag{5}$$

where $O_{1,i}$ and $O_{1,j}$ denote the output functions and $\mu_{\text{A}i}$ and $\mu_{\text{B}i}$ denote the membership functions. In stage 2, it consists of two nodes labeled Π. The output $W1$ and $W2$ are the weight functions of the next layer. The output of this stage is the product of the input signal, which is defined as follows

$$O_{1,i} = w_i = \mu_{\text{A}i}(x)\mu_{\text{B}i}(y), i = 1, 2 \tag{6}$$

where $O_{2,i}$ is the output of stage 2.

In stage 3, nodes are labeled N. The function of this stage is to normalize the weight function in the following process

$$O_{3,i} = \overline{w}_i = \frac{w_i}{w_1 + w_2}, i = 1, 2 \tag{7}$$

where $O_{3,i}$ is the output of stage 3. In stage 4, defuzzification is realized. The nodes are adaptive nodes. The relationship can be defined as the following

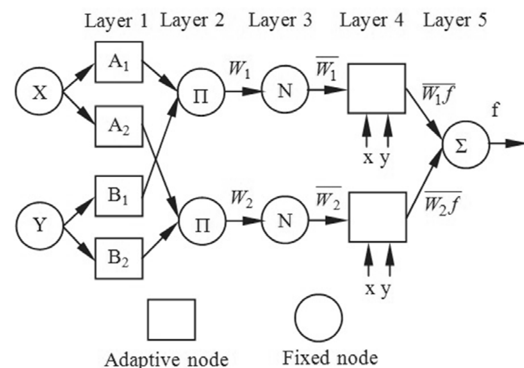

Figure 2. ANFIS architecture.

© 2023 Wiley-VCH GmbH

$$O_{4,i} = \overline{w}_i(p_i x + q_i y + r_i), i = 1, 2 \quad (8)$$

where $O_{4,i}$ is output of stage 4. And p_i, q_i, and r_i are the linear parameters of the node.

In stage 5, node is labeled as Σ. The output is composed of all the ingredients of the inputs, which represents the results of cleaning rates. The output can be expressed as follows

$$O_{5,i} = \sum_i \overline{w}_i f_i = \frac{\sum_i w_i f_i}{\sum_i w_i}, i = 1, 2 \quad (9)$$

where $O_{5,i}$ is the output of stage 5.

2.3. Parameter Estimation from *I–V* Characteristic of SBD

2.3.1. Parameter Estimation Problem and Objective Function

The general *I–V* formula of SBD can be suggested as[23,26,40]

$$I = AA^* T^2 \exp\left(-\frac{q\phi_b}{kT}\right)\left[\exp\left(\frac{q(V - IR_s)}{nkT}\right) - 1\right] \quad (10)$$

where $AA^* T^2 \exp\left(-\frac{q\phi_b}{kT}\right)$ is the saturation current I_0. A^* is the effective Richardson constant and equals to 8.16 A cm^{-2} K^2 for n-type GaAs, A is the diode area ($1{,}767 \times 10^{-2}$ cm), and T is the ambient temperature in Kelvin. n is a measure of the diode's fitness for pure thermionic emission. It should ideally be equal to one. However, the value of n usually has a value greater than one. Voltage and current of diode terminal are V and I, respectively.

An artificial intelligence optimization algorithm needs an objective function to solve the desired problem. The objective function is a mathematical model consisting of the parameters to be found. In particular, the optimization algorithm finds the desired parameters by minimizing the defined objective function. Here, using Equation (10), the objective function can be constructed as follows for parameter estimation of Ni/n-GaAs/In SBD.[26,40]

$$\mathrm{Obj}(F(I_{\exp}, V_{\exp}, P_{\mathrm{est}})) = \mathrm{RMSE}\left(I_{\exp} - AA^* T^2 \exp\left(-\frac{q\phi_b}{kT}\right)\left[\exp\left(\frac{q(V_{\exp} - I_{\exp}R_s)}{nkT}\right) - 1\right]\right) \quad (11)$$

where $I_{\exp}$ and $V_{\exp}$ are the experimental current and voltage values. R_s is the neutral region resistance. The unit of objective function is current. In this study, the MA algorithm optimized the desired n, ϕ_b, and R_s values by minimizing the objective function using the measured current and voltage values.

2.3.2. MA

Zervoudakis and Tsafarakis proposed MA in 2020.[41] This algorithm is an artificial intelligence algorithm that models the mating and flight styles of mayfly insects. The MA has been very successful in solving many optimization problems. In particular, it has shown a very good solution performance compared with many optimization algorithms in the problem of estimating the parameters of solar cells by many researchers and practitioners. The pseudocode structure of the MA algorithm is given in **Figure 3**.

3. Results and Discussion

In this section, the results and discussions are examined in two separate sections as the modeling of the Ni/n-GaAs/In SBD and the estimation of its electrical parameters. In the modeling, for the varying annealing temperatures, the performances of all the regression methods were analyzed in training and testing phases. Performance indicators are tabulated and the comparison figures are demonstrated for aforementioned situations. In the estimation, for annealing temperatures of 200, 300, 400, 500, 600, and 350 °C, the electrical parameters of SBD were estimated from the *I–V* characteristics by using MA. In particular, the *I–V* data of 350 °C were produced from the proposed regression model of SBD without experimental procedure. And this is taken into account in parameter estimation. In this study, regression models and electrical parameter estimation were developed with the aid of MATLAB platform. All computational procedures were performed on a computer with Intel(R) Core(TM) i5 processor, 8 GB Ram and Windows 10 software.

3.1. Modeling of Ni/n-GaAs/In SBD

Ni/n-GaAs SBD contacts were fabricated and annealed from temperature of 200 °C up to 600 °C with 100 °C steps. For each annealing temperature, voltage source was applied to the contacts from −1 to +0.5 V with 0.005 V steps. Measured *I–V* data were recorded. In total, 1503 *I–V* data were recorded. When 1203 data were randomly allocated for training, 300 data were selected for testing. In all regression models, when voltage and annealing temperature data were determined as inputs data, diode current data were defined as output data. In **Table 1**, calculated RMSE, MSE, and MAE values of all linear regression methods were shown for both training and testing phases. Also, *R* values were tabulated.

Basic (BLR), interactions (ILR), robust (RLR), and stepwise (SLR) regressions were the LR methods and they were used in the modeling of SBD using training and test data. ILR and SLR achieved same error values and their performances were better than those of the BLR and RLR. For ILR and SLR, when RMSE, MSE, MAE, and R were 1.8956e-04, 3.5932e-08, 8.6338e-05, and 0.4263 for training, they were 1.8439e-04, 3.4000e-08, 8.5468e-05, and 0.4294 for test, respectively. In general, when RMSE values decreased to zero, *R* values increased to one. Then, fine tree (FTR), medium tree (MTR), and coarse tree (CTR) regressions were applied. When FTR achieved good estimation results, MTR and CTR showed worse performance. For FTR, when RMSE, MSE, MAE, and *R* were 2.2429e-05, 5.0304e-10, 5.1910e-06, and 0.9943 for training, they were 2.9596e-05, 8.7591e-10, 6.5527e-6, and 0.9894 for test, respectively. SVM algorithms with linear (LSVM), fine Gaussian (FGSVM), medium Gaussian (MGSVM), and coarse Gaussian (CGSVM) kernels were implemented for the modeling of

© 2023 Wiley-VCH GmbH

18626319, 2023, 6, Downloaded from https://onlinelibrary.wiley.com/doi/10.1002/pssa.202200740 by Cumhuriyet University, Wiley Online Library on [10/01/2024]. See the Terms and Conditions (https://onlinelibrary.wiley.com/terms-and-conditions) on Wiley Online Library for rules of use; OA articles are governed by the applicable Creative Commons License

18626319, 2023, 6, Downloaded from https://onlinelibrary.wiley.com/doi/10.1002/pssa.202200740 by Cumhuriyet University, Wiley Online Library on [10/01/2024]. See the Terms and Conditions (https://onlinelibrary.wiley.com/terms-and-conditions) on Wiley Online Library for rules of use; OA articles are governed by the applicable Creative Commons License

Algorithm: Pseudo-code of Mayfly Algorithm

```
1: Load I-V data of SBD, Setup control parameter, problem dimensions and bounds
2: Generate the male mayflies population and their velocities
3: Generate the female mayflies population and their velocities
4: Evaluate solutions applying predefined objective functions in Equation 11.
5: Calculate global best (gbest) and personal best (pbest)
6: while (stopping criteria)
7:     Update velocities and position of males and females mayflies according to velocity and
       position limits
8:     Evaluate solutions applying predefined objective functions
9:     Rank mayflies population
10:    Mate mayflies population
11:    Evaluate offspring
12:    Separate randomly the offspring to male and female
13:    Replace worst solutions with the best new solutions
14:    Update pbest and gbest
15: end while
16: Save best solution population
    Determine electrical parameter of SBD
    Calculate error function
    Plot I-V characteristic of SBD
```

Figure 3. Pseudocode of MA for parameter estimation of Ni/n-GaAs/In SBD.

SBD. FGSVM obtained best error values. For FGSVM, when RMSE, MSE, MAE, and R were 9.7843e-07, 9.5732e-13, 8.1908e-07, and 0.9999 for training, they were 9.7343e-07, 9.4756e-13, 8.1845e-07, and 0.9999 for test, respectively. The fine Gaussian kernel improved the performance of SVM compared to others. As suggested in the literature,[20] SVM with Gaussian kernel has a good performance for the modeling of SBD compared to the other SVM kernels. Rational quadratic (RQGPR), squared exponential (SEGPR), exponential (EGPR), matern 5/2 (M5/2GPR), and matern (M3/2GPR) were the kernels of GPR. Each kernel was again applied to the aforementioned rules for the modeling of SBD. In general, proposed kernels performed similarly, but M3/2GPR was achieved best results. For M3/2GPR, when RMSE, MSE, MAE, and R were 1.9433e-04, 3.7764e-08, 7.0092e-05, and 0.3779 for training, they were 1.8838e-04, 3.5488e-08, 6.9204e-05, and 0.3820 for test, respectively. Ensemble boosted tree (EBOT) and bootstrap-aggregated tree (EBAT) regression were employed. For EBOT, RMSE, MSE, MAE, and R were 2.5319e-05, 6.4104e-10, 3.9802e-06, and 0.9927 for training, they were 2.1918e-05, 4.8041e-10, 5.3415e-06, and 0.9942 for test, respectively. The best error values among all algorithms were obtained with the ANFIS model. When RMSE, MSE, MAE, and R were 6.0341e-07, 3.6410e-13, 2.3873e-07, and 0.9999 for training, they were 5.8904e-07, 3.4697e-13, 2.3083e-07, and 0.9999 for test. In the previous study by Torun and Dogan, for ANFIS, when RMSE, MSE, and MAE were obtained 6.806e-06, 4.632e-11, and 3.914e-06 for test, they were achieved 6.231e-06, 3.883e-11, and 3.782e-06 for train, respectively.[20] According to these results, ANFIS reached small error values in two different modeling studies of SBD compared to other regression methods. In aforementioned study, room temperature is changed between 40 and 400 K. And, in this study, annealing temperature is changed between 200 and 600 °C. Also, in this article, for ANFIS, grid partitioning was used to generate fuzzy inference system from the measured I–V data and generalized bell-shaped membership function was chosen. In the other aforementioned study, subtractive clustering with 0.25 radii was applied for ANFIS.

As seen from the results, when all competitor regression methods were compared, the ranking of performances was ANFIS/FGSVM, FTR, EBOT, MGSVM, EBAT, MTR, CTR, CGSVM, SLR/ILR, BLR, M3/2GPR, RQGPR/EGPR/M5/2GPR/SEGPR, LSVM, and RLR. Although the aforementioned regression methods have different application conditions and complexities, this ordering shows that each of the methods achieved different results for the modeling of SBD. For example, although FGSVM is a variant of SVM, it performed better than other SVM types and was in second place after the ANFIS method. This is the explanation why the comparison table of all regression methods is given in such detail for training and test phases.

 © 2023 Wiley-VCH GmbH

18626319, 2023, 6, Downloaded from https://onlinelibrary.wiley.com/doi/10.1002/pssa.202200740 by Cumhuriyet University, Wiley Online Library on [10/01/2024]. See the Terms and Conditions (https://onlinelibrary.wiley.com/terms-and-conditions) on Wiley Online Library for rules of use; OA articles are governed by the applicable Creative Commons License

Table 1. Performance comparison of regression methods for SBD.

Model		Training				Test			
		RMSE [A]	MSE [A]	MAE [A]	*R*	RMSE [A]	MSE [A]	MAE [A]	*R*
	ANFIS	6.0341e-07	3.6410e-13	2.3873e-07	0.9999	5.8904e-07	3.4697e-13	2.3083e-07	0.9999
Linear regression	BLR	1.9170e-04	3.6750e-08	8.8520e-05	0.4072	1.8609e-04	3.4631e-08	8.7541e-05	0.4081
	ILR	1.8956e-04	3.5932e-08	8.6338e-05	0.4263	1.8439e-04	3.4000e-08	8.5468e-05	0.4294
	RLR	2.0989e-04	4.4054e-08	4.3604e-05	0.0011	2.0384e-04	4.1552e-08	4.2638e-05	0.0011
	SLR	1.8956e-04	3.5932e-08	8.6338e-05	0.4263	1.8439e-04	3.4000e-08	8.5468e-05	0.4294
Trees regression	FTR	2.2429e-05	5.0304e-10	5.1910e-06	0.9943	2.9596e-05	8.7591e-10	6.5527e-06	0.9894
	MTR	5.8365e-05	3.4065e-09	1.0951e-05	0.9606	5.4362e-05	2.9552e-09	1.2757e-05	0.9638
	CTR	1.1898e-04	1.4157e-08	2.4821e-05	0.8238	1.2345e-04	1.5241e-08	2.8452e-05	0.7957
Support vector machines	LSVM	2.0596e-04	4.2418e-08	1.0901e-04	0.1841	2.0036e-04	4.0144e-08	1.0773e-04	0.1928
	FGSVM	9.7843e-07	9.5732e-13	8.1908e-07	0.9999	9.7343e-07	9.4756e-13	8.1845e-07	0.9999
	MGSVM	3.5578e-05	1.2658e-09	1.3987e-05	0.9855	3.4373e-05	1.1815e-09	1.4028e-05	0.9857
	CGSVM	1.6794e-04	2.8202e-08	3.7724e-05	0.5999	1.6267e-04	2.6461e-08	3.6971e-05	0.6027
Ensemble trees	EBOT	2.5319e-05	6.4104e-10	3.9802e-06	0.9927	2.1918e-05	4.8041e-10	5.3415e-06	0.9942
	EBAT	5.3900e-05	2.9052e-09	1.3602e-05	0.9701	4.7521e-05	2.2582e-09	1.2749e-05	0.9725
Gaussian process regression	SEGPR	2.0531e-04	4.2153e-08	7.8023e-05	0.2078	1.9934e-04	3.9735e-08	7.7029e-05	0.2091
	M5/2GPR	2.0531e-04	4.2152e-08	7.8023e-05	0.2078	1.9934e-04	3.9735e-08	7.7029e-05	0.2091
	EGPR	2.0531e-04	4.2153e-08	7.8023e-05	0.2078	1.9934e-04	3.9735e-08	7.7029e-05	0.2091
	RQGPR	2.0531e-04	4.2153e-08	7.8023e-05	0.2078	1.9934e-04	3.9735e-08	7.7029e-05	0.2091
	M3/2GPR	1.9433e-04	3.7764e-08	7.0092e-05	0.3779	1.8838e-04	3.5488e-08	6.9204e-05	0.3820

For train and test stages, current-annealing temperature overlap charts of experimental data versus outputs of competitor algorithms are shown in **Figure 4–9**. Especially here, ANFIS, SLR, FTR, FGSVM, EBOT, and M3/2GPR were determined and their graphs were drawn because the approaches that gave the best results in their subgroups were preferred. As shown in Figure 4 and 7, in both training and testing stages, the outputs of the FGSVM and ANFIS coincided with the experimental currents in all annealing temperature. Low RMSE, MSE, and MAE values of models affected positively the agreement between experimental data and outputs for each annealing temperature. Low error values and high *R* value increased model performance. However, in terms of overlap, FTR and EBOT performed moderately as shown in Figure 6 and 8, while SLR and M3/2GPR performed poorly as shown in Figure 5 and 9.

Current-sample curves of experimental current versus output currents of competitor algorithms are shown in **Figure 10–15** for train and test phases. Error differences between experimental and output current data in these figures supported aforementioned performance comparisons for ANFIS, SLR, FTR,

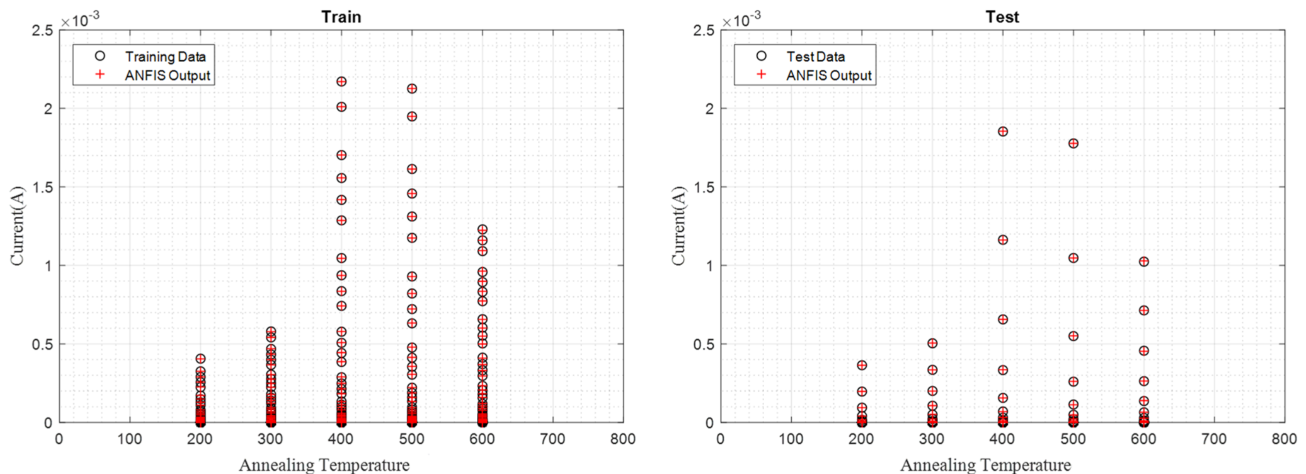

Figure 4. Current-annealing temperature overlap chart of experimental data versus ANFIS output for train and test phases.

© 2023 Wiley-VCH GmbH

18626319, 2023, 6, Downloaded from https://onlinelibrary.wiley.com/doi/10.1002/pssa.202200740 by Cumhuriyet University, Wiley Online Library on [10/01/2024]. See the Terms and Conditions (https://onlinelibrary.wiley.com/terms-and-conditions) on Wiley Online Library for rules of use; OA articles are governed by the applicable Creative Commons License

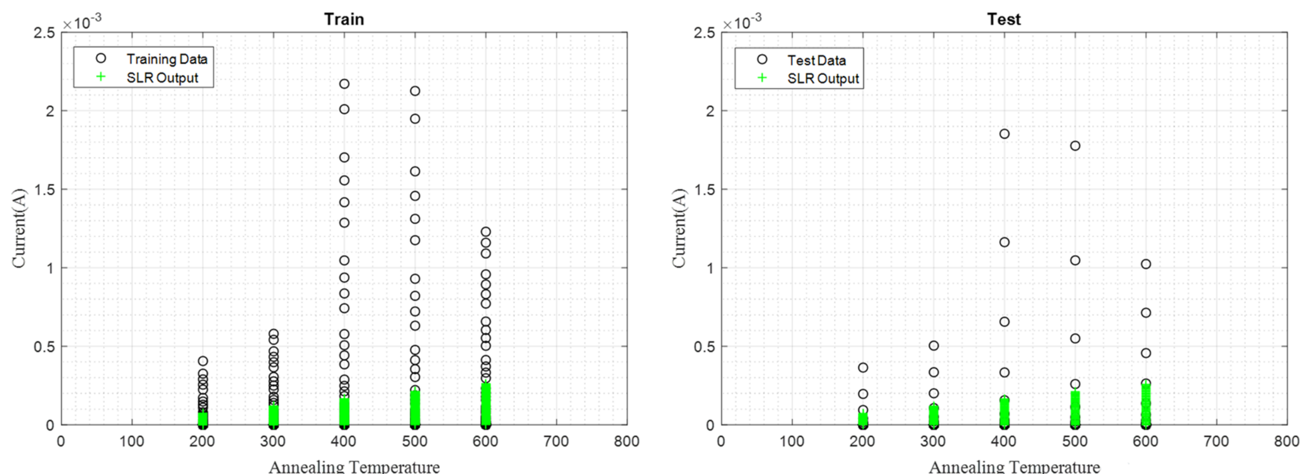

Figure 5. Current-annealing temperature overlap chart of experimental data versus SLR output for train and test phases.

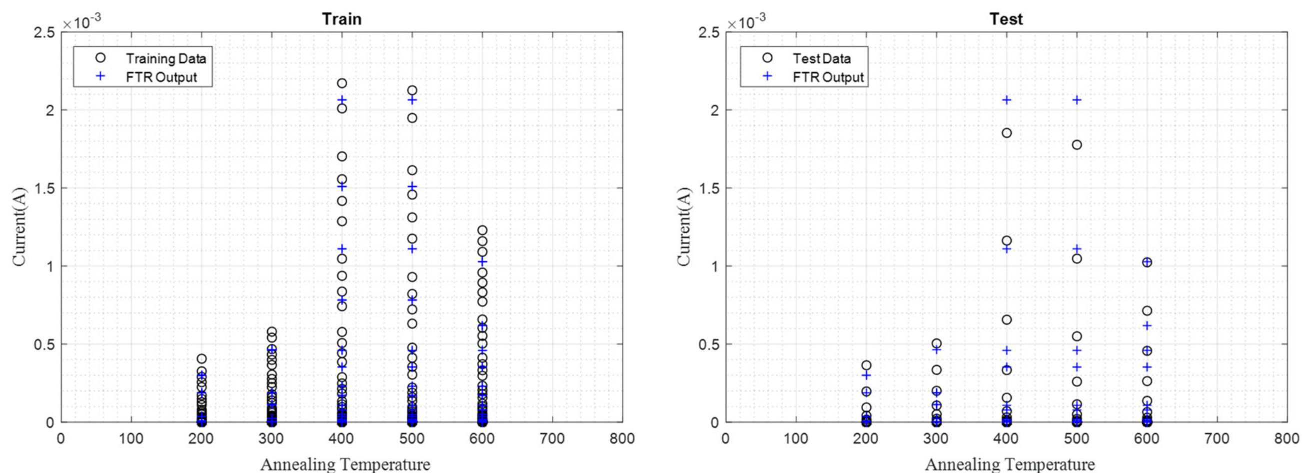

Figure 6. Current-annealing temperature overlap chart of experimental data versus FTR output for train and test phases.

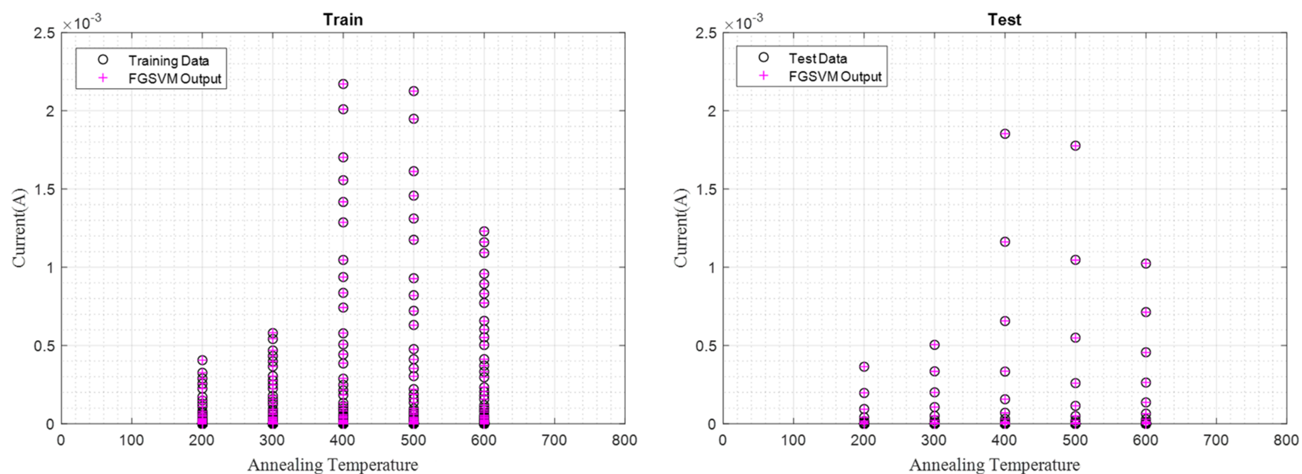

Figure 7. Current-annealing temperature overlap chart of experimental data versus FGSVM output for train and test phases.

 © 2023 Wiley-VCH GmbH

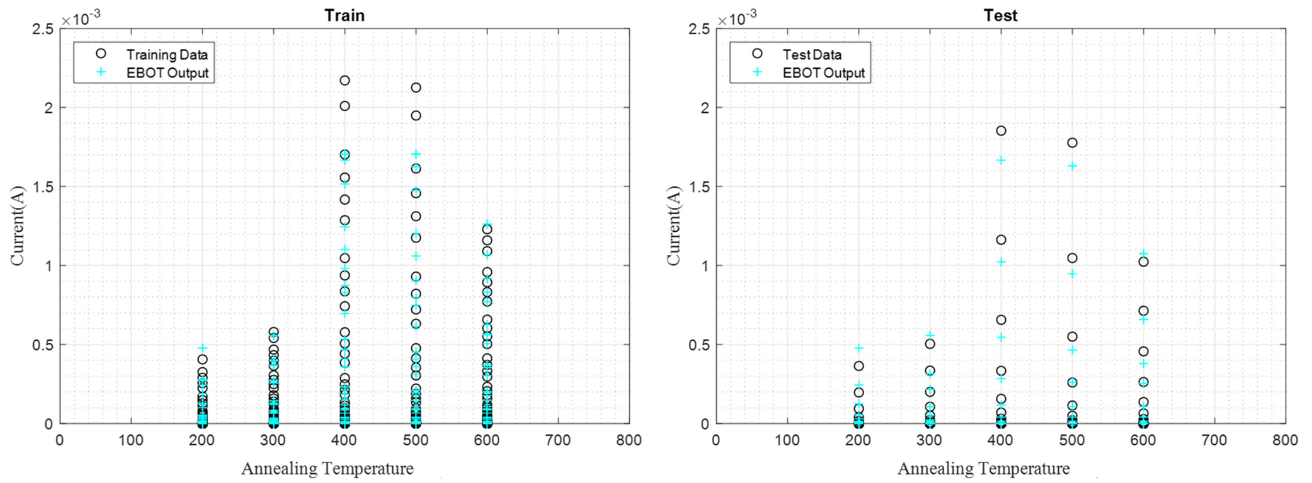

Figure 8. Current-annealing temperature overlap chart of experimental data versus EBOT output for train and test phases.

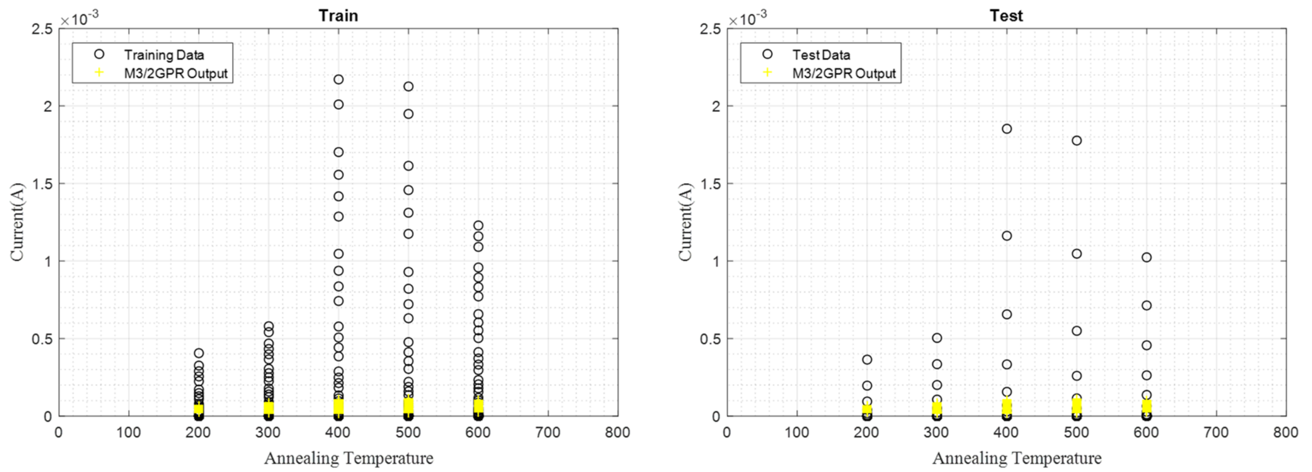

Figure 9. Current-annealing temperature overlap chart of experimental data versus M3/2GPR output for train and test phases.

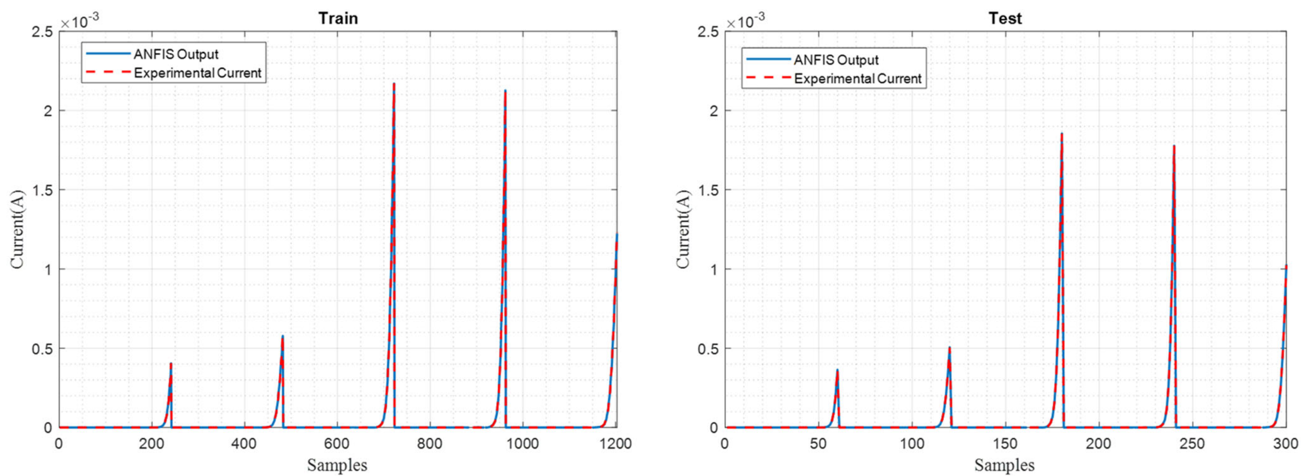

Figure 10. Current-sample curves of experimental current versus ANFIS output current for train and test phases.

© 2023 Wiley-VCH GmbH

18626319, 2023, 6, Downloaded from https://onlinelibrary.wiley.com/doi/10.1002/pssa.202200740 by Cumhuriyet University, Wiley Online Library on [10/01/2024]. See the Terms and Conditions (https://onlinelibrary.wiley.com/terms-and-conditions) on Wiley Online Library for rules of use; OA articles are governed by the applicable Creative Commons License

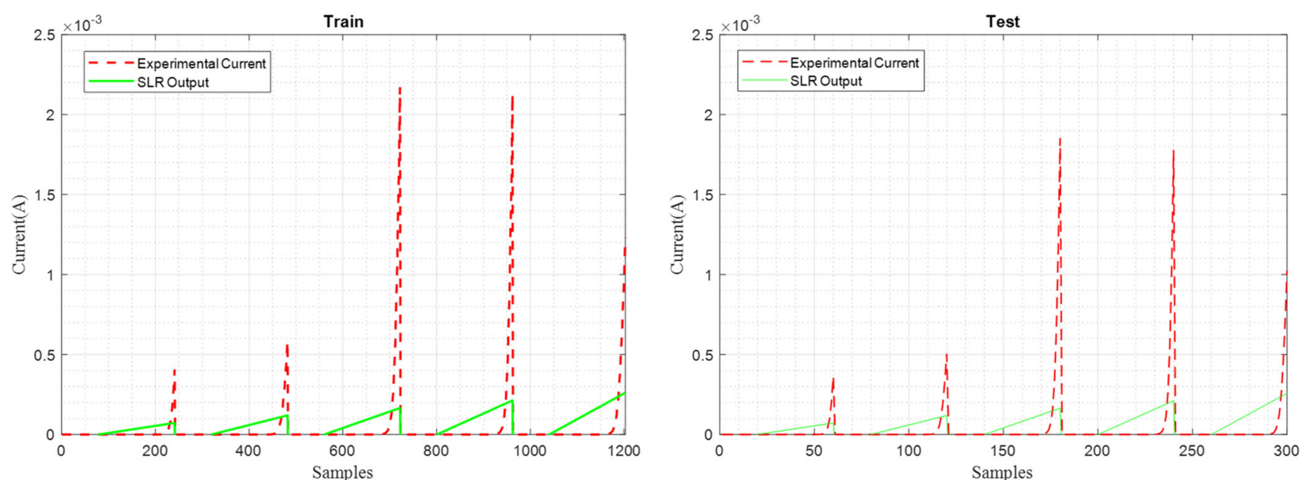

Figure 11. Current-sample curves of experimental current versus SLR output current for train and test phases.

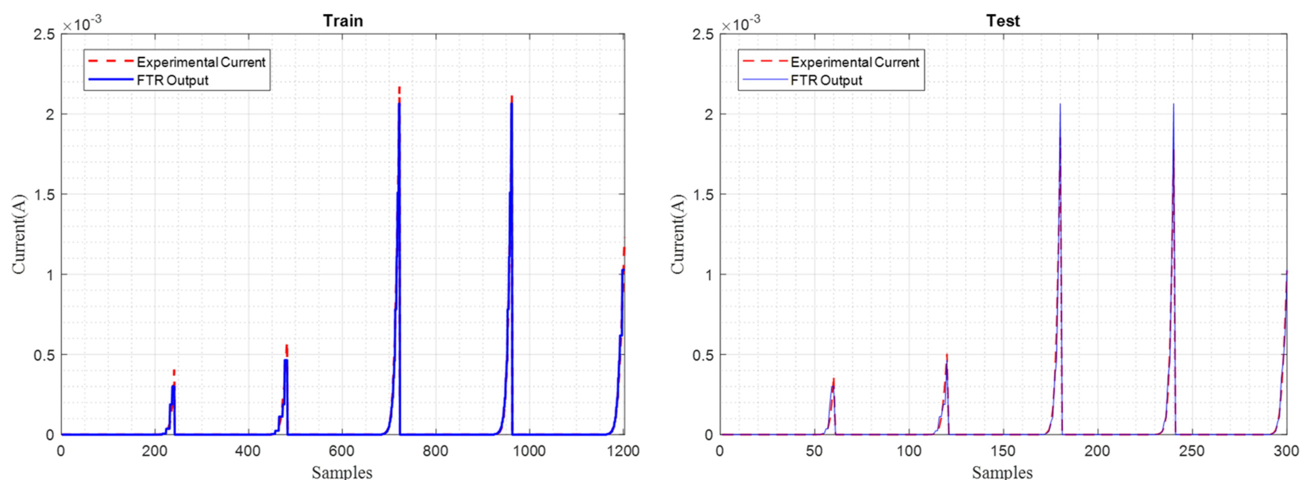

Figure 12. Current-sample curves of experimental current versus FTR output current for train and test phases.

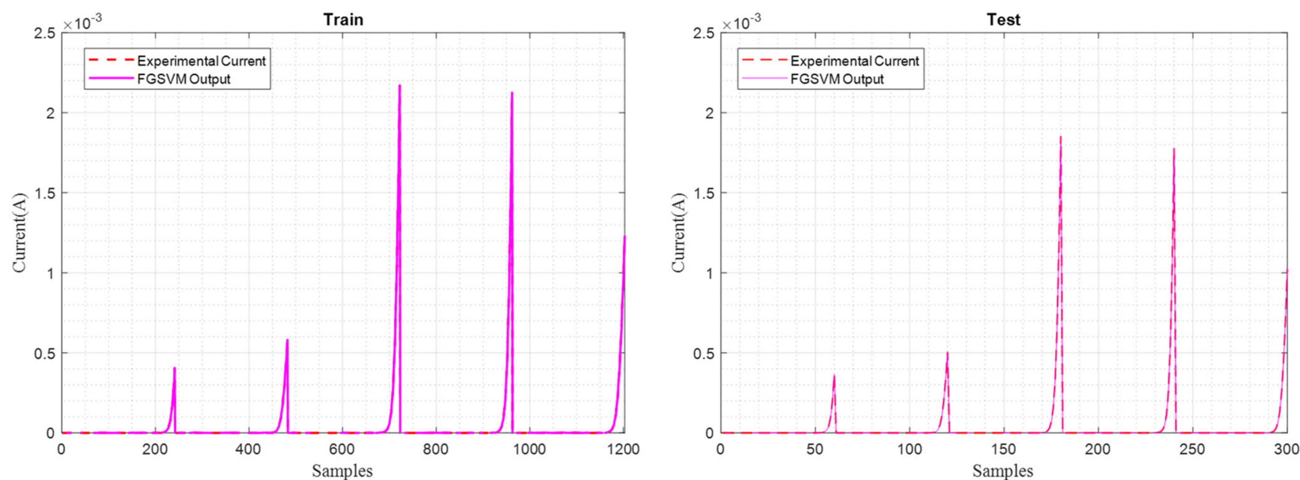

Figure 13. Current-sample curves of experimental current versus FGSVM output current for train and test phases.

© 2023 Wiley-VCH GmbH

18626319, 2023, 6, Downloaded from https://onlinelibrary.wiley.com/doi/10.1002/pssa.202200740 by Cumhuriyet University, Wiley Online Library on [10/01/2024]. See the Terms and Conditions (https://onlinelibrary.wiley.com/terms-and-conditions) on Wiley Online Library for rules of use; OA articles are governed by the applicable Creative Commons License

18626319, 2023, 6, Downloaded from https://onlinelibrary.wiley.com/doi/10.1002/pssa.202200740 by Cumhuriyet University, Wiley Online Library on [10/01/2024]. See the Terms and Conditions (https://onlinelibrary.wiley.com/terms-and-conditions) on Wiley Online Library for rules of use; OA articles are governed by the applicable Creative Commons License

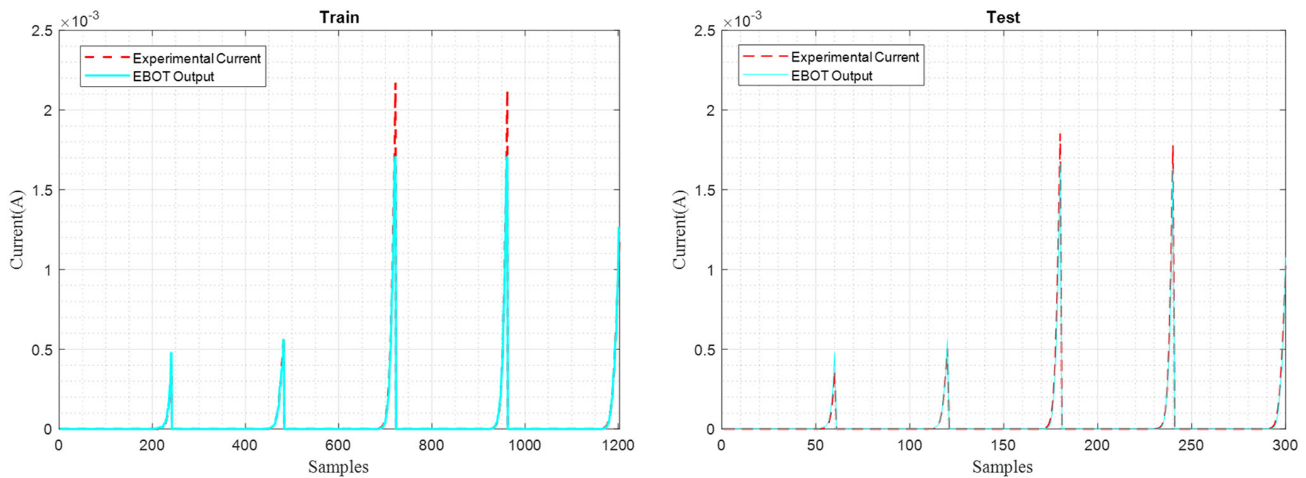

Figure 14. Current-sample curves of experimental current versus EBOT output current for train and test phases.

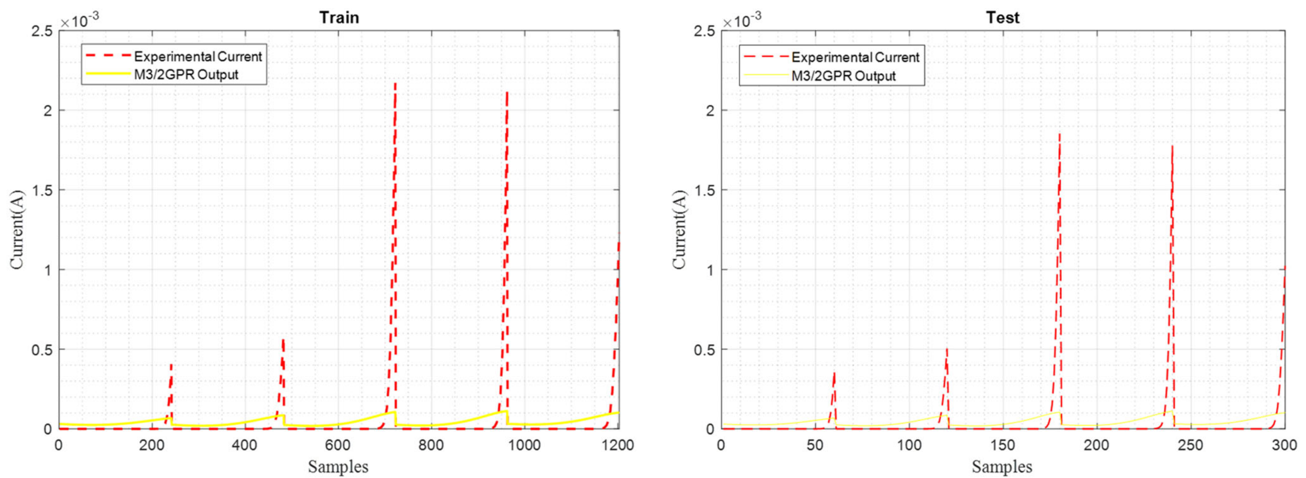

Figure 15. Current-sample curves of experimental current versus M3/2GPR output current for train and test phases.

FGSVM, EBOT, and M3/2GPR methods. In Figure 10 and 13, the outputs of ANFIS and FGSVM overlapped completely with the experimental current because of the low RMSE and high R values. As shown in Figure 11, 12, 14, and 15, the overlap performances of the other methods were lower than those of the ANFIS and FGSVM because their RMSE error values were about e-05 levels. As a result, low RMSE and high R values reduced the difference between the experimental current and outputs of competitor algorithms.

For train and test phases, **Figure 16–20** showed the $I–V$ curves of competitor algorithms for annealing temperatures of 200, 300, 400, 500, and 600 °C. As can be seen from these figures and can be understood from the error function values in Table 1, the output performances of ANFIS and FGSVM are quite good compared with those of other proposed models for the varying annealing temperature. As a result, this situation showed the robustness of the ANFIS and FGSVM methods. On the other hand, SLR, FTR, EBOT, and M3/2GPR methods could not follow the experimental $I–V$ data curve for all annealing temperatures.

3.2. Parameter Estimation of SBD

In the previous section, 19 different regression methods were compared and it was seen that the best performance was exhibited by the ANFIS method. In this section, n, ϕ_b, and R_s values, which were electrical characteristic parameters, were estimated by MA using $I–V$ data of Ni/nGaAs SBDs for annealing temperatures of 200, 300, 400, 500, and 600 °C. In addition, unlike similar studies in the literature, $I–V$ data for the annealing temperature of 350 °C were produced and parameter estimation was performed from this characteristic and added to the comparison table. n, ϕ_b, and R_s characterize the behavior of Ni/n-GaAs SBD. Therefore, it is important to estimate these parameters from the $I–V$ data all at once. The characteristic parameters estimated from the $I–V$ data for each annealing temperature using the MA are shown in **Table 2**. Herein, the RMSE error value for each estimation operation was quite small. This shows that the MA makes a precise estimation. Likewise, the excellent fit between the experimental and estimation data in **Figure 21** supported this

© 2023 Wiley-VCH GmbH

18626319, 2023, 6, Downloaded from https://onlinelibrary.wiley.com/doi/10.1002/pssa.202200740 by Cumhuriyet University, Wiley Online Library on [10/01/2024]. See the Terms and Conditions (https://onlinelibrary.wiley.com/terms-and-conditions) on Wiley Online Library for rules of use; OA articles are governed by the applicable Creative Commons License

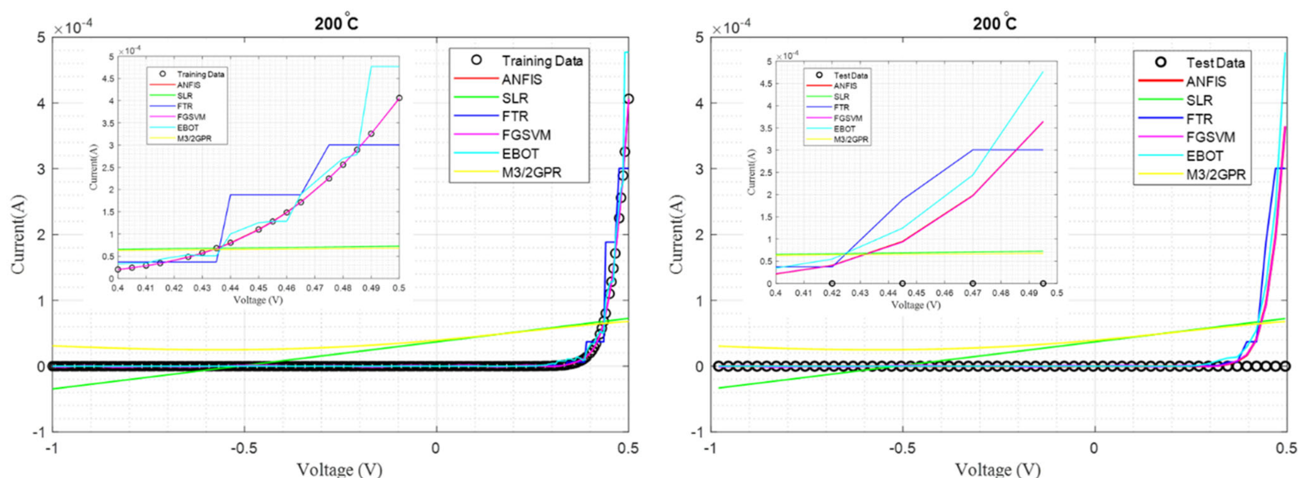

Figure 16. *I–V* curves of ANFIS, SLR, FTR, FGSVM, EBOT, and M3/2GPR for 200 °C annealing temperature.

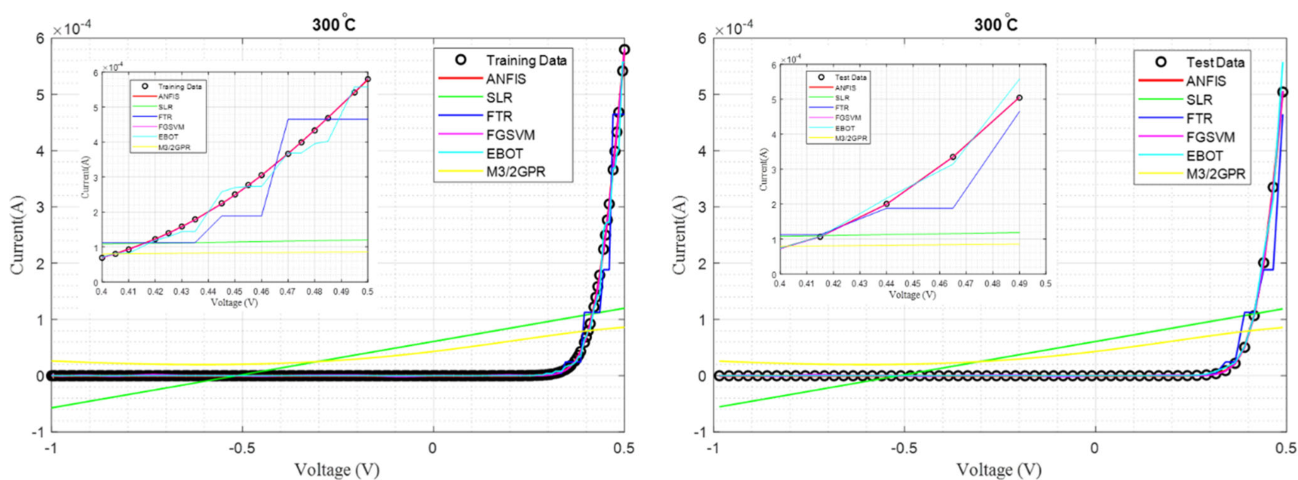

Figure 17. *I–V* curves of ANFIS, SLR, FTR, FGSVM, EBOT, and M3/2GPR for 300 °C annealing temperature.

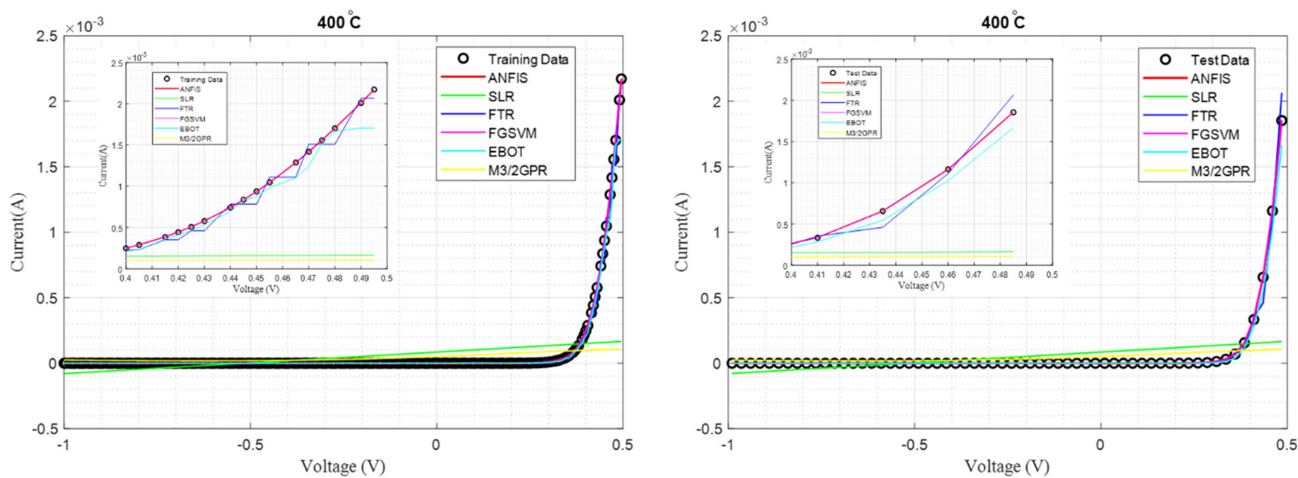

Figure 18. *I–V* curves of ANFIS, SLR, FTR, FGSVM, EBOT, and M3/2GPR for 400 °C annealing temperature.

© 2023 Wiley-VCH GmbH

18626319, 2023, 6, Downloaded from https://onlinelibrary.wiley.com/doi/10.1002/pssa.202200740 by Cumhuriyet University, Wiley Online Library on [10/01/2024]. See the Terms and Conditions (https://onlinelibrary.wiley.com/terms-and-conditions) on Wiley Online Library for rules of use; OA articles are governed by the applicable Creative Commons License

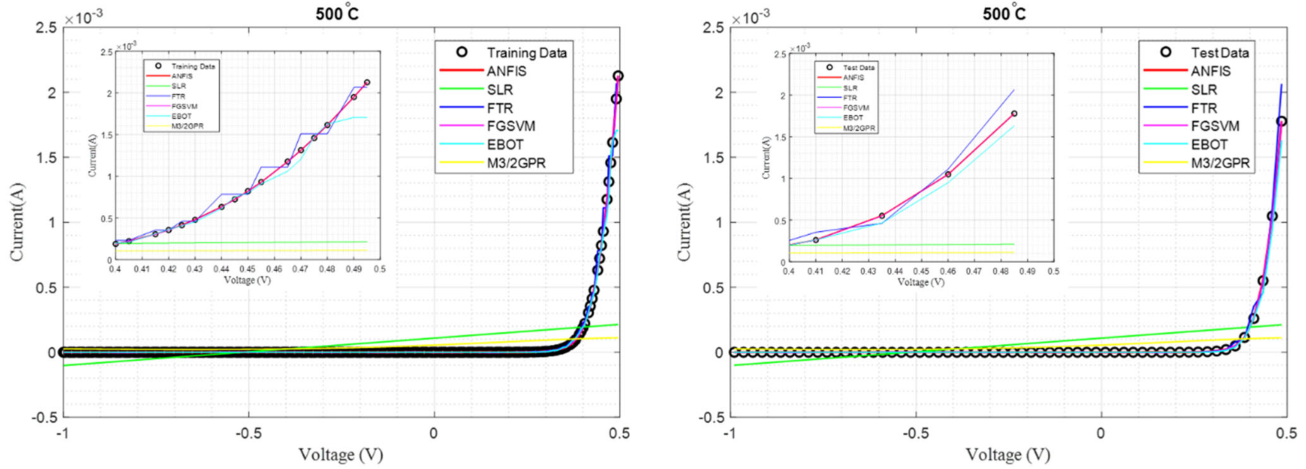

Figure 19. *I–V* curves of ANFIS, SLR, FTR, FGSVM, EBOT, and M3/2GPR for 500 °C annealing temperature.

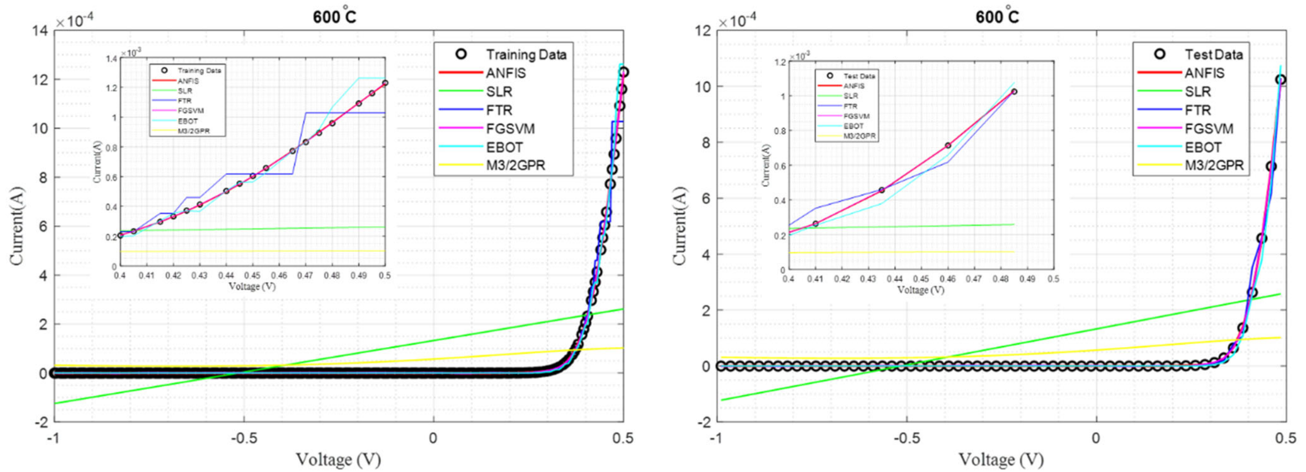

Figure 20. *I–V* curves of ANFIS, SLR, FTR, FGSVM, EBOT, and M3/2GPR for 600 °C annealing temperature.

Table 2. Estimated characteristic parameter of SBD using MA..

	Annealing temperature [°C]					
	200	300	350	400	500	600
n	1.0519	1.0705	1.2222	1.1335	1.0931	1.1314
ϕ_b [eV]	0.8963	0.8541	0.8026	0.8022	0.8236	0.8029
R_s [Ω]	50.4329	81.8431	49.2221	16.7509	14.1174	47.0793
RMSE [A]	7.0499e-08	1.3861e-07	1.0406e-06	8.9686e-07	8.4819e-07	2.4192e-07

suggestion. Especially, the overlaps in the series resistance regions were remarkable. Also, as shown in Table 2, thermal annealing process changed the electrical characteristic parameters of the SBD. Thus, the effect of thermal annealing has been proven in the production of SBD with the desired quality interface and performance. For MA simulation, population size male and female mayflies, iteration, inertia weight, and nuptial dance were experimentally selected 20, 500, 0.8, and 5, respectively.[41] Personal and global learning coefficients were determined 1 and 1.5. The MA algorithm was run 50 times with the selected algorithm parameters and the best values were tabulated.

4. Conclusion

In this article, a three-stage study was carried out for the Ni/n-GaAs SBD. In the first stage, SBDs were produced. Then, they were annealed from annealing temperatures of 200, 300, 400, 500, and 600 °C. For each annealing temperature,

 © 2023 Wiley-VCH GmbH

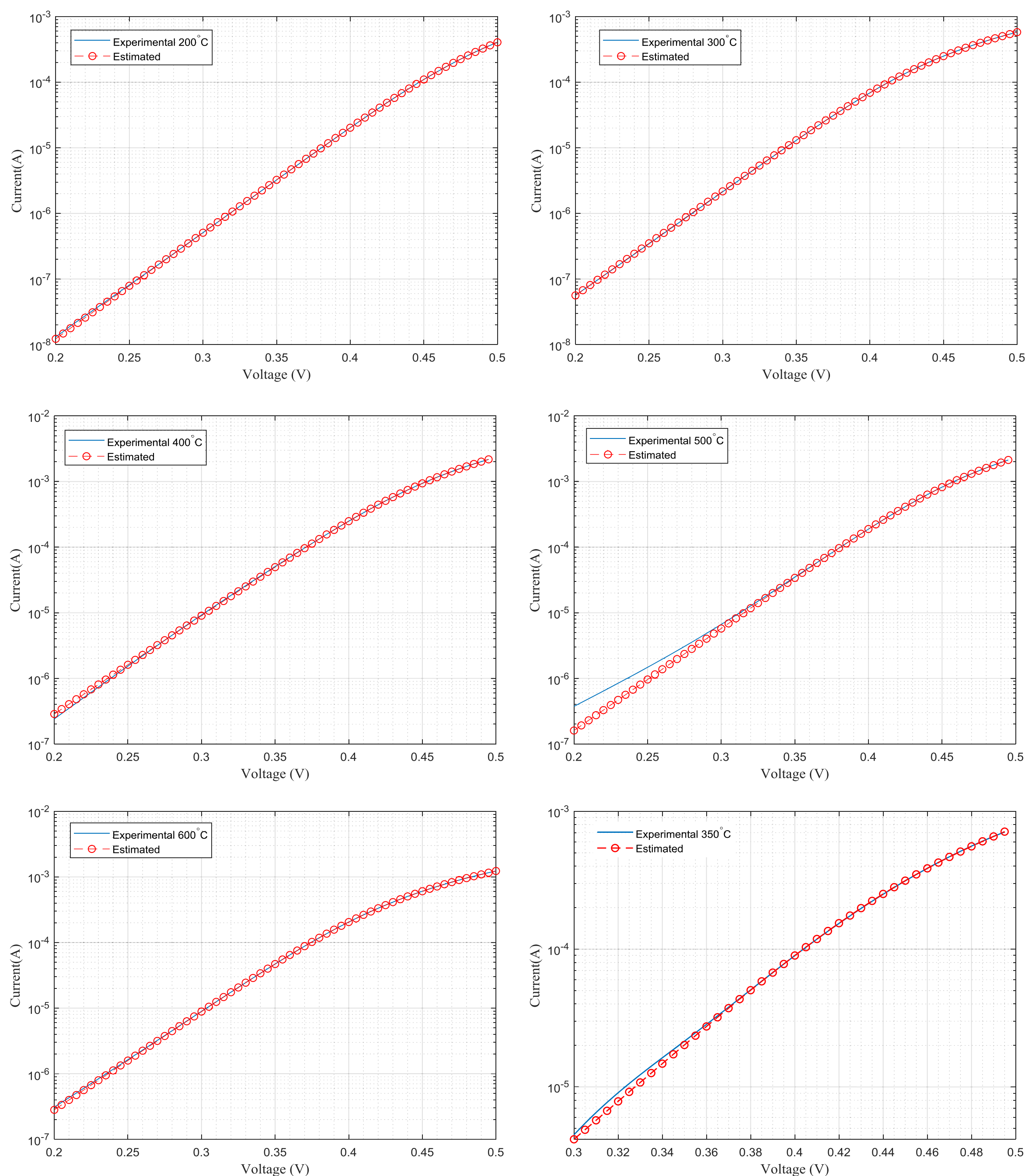

Figure 21. Experimental versus estimated *I–V* data for 200, 300, 350, 400, 500, and 600 °C.

voltage source was applied to the contacts from −1 to +0.5 V with 0.005 V steps. The *I–V* data of SBDs were recorded. In total, 1503 *I–V* data were obtained. In the second stage, when 1203 data were selected for training, 300 data were determined for testing. While the *I–V* data were divided into train and test data, one out of every five data was reserved as a test data. Thus, a qualified sampling was made, which increased the all model performance. Then, using this training and test data, *I–V* characteristic models of SBDs were created with the aid of 19 different regression methods. All models were evaluated using RMSE, MSE, MAE, and *R* formulas. The lowest error values were achieved for the ANFIS and the FGSVM model. Thus, *I–V* characteristic model of ANFIS was created that can accurately generate the diode current corresponding to the desired temperature or voltage. In addition, *I–V* data for the annealing temperature of 350 °C were produced using this model. In the third stage, the estimation of electrical characteristic parameter was made using the *I–V* data for annealing temperatures of 200, 300, 350, 400, 500, and 600 °C. n, ϕ_b, and R_s values were found with high precision using the MA. As a result, an estimation approach was alternatively

 © 2023 Wiley-VCH GmbH

18626319, 2023, 6, Downloaded from https://onlinelibrary.wiley.com/doi/10.1002/pssa.202200740 by Cumhuriyet University, Wiley Online Library on [10/01/2024]. See the Terms and Conditions (https://onlinelibrary.wiley.com/terms-and-conditions) on Wiley Online Library for rules of use; OA articles are governed by the applicable Creative Commons License

applied by the MA. Thus, for researchers and practitioners, the experimental, modeling, and estimation stages were applied to realize a result-oriented key solution study in in the light of all scientific results.

Acknowledgements

The authors would like to thank Prof. Dr. Abdülmecit Türüt for her assistance in the production and all measurement stages of the Ni/n-GaAs/In Schottky Barrier diode. The authors also thank all reviewers for their constructive comments.

Conflict of Interest

The authors declare no conflict of interest.

Data Availability Statement

The data that support the findings of this study are available from the corresponding author upon reasonable request.

Keywords

mayfly algorithm, parameter estimation, regression, schottky barrier diodes

Received: October 31, 2022
Revised: January 3, 2023
Published online: February 5, 2023

[1] A. Türüt, B. Batı, A. Kökçe, M. Sağlam, N. Yalçın, *Scripta* **1996**, *53*118.
[2] J. Bardeen, *Phys. Rev.* **1947**, *71*, 717.
[3] S. M. Sze, D. C. Mattis, *Phys. Today* **1970**, *23*, 75.
[4] G. Y. Robinson, *Physics and Chemistry of III–V Compound Semiconductor Interfaces* (Ed: C.W. Wilmsen), Plenum Press, New York **1985**, pp. 73–163, https://doi.org/10.1007/978-1-4684-4835-1.
[5] R. L. Van Meirhaeghe, W. H. Laflere, F. Cardon, *J. Appl. Phys.* **1994**, *76*, 403.
[6] E. H. Rhoderick, R. H. Williams, *Metal–Semiconductor Contacts*, Clarendon Press, Oxford **1988**.
[7] M. Sağlam, A. Türüt, *Semicond. Sci. Technol.* **1997**, *12*1028.
[8] N. Yıldırım, A. Türüt, H. Dogan, *Surf. Rev. Lett.* **2018**, *25*1850082.
[9] H. Doğan, N. Yıldırım, A. Turut, *Microelectron. Eng.* **2008**, *85*655.
[10] S. K. Cheung, N. W. Cheung, *Appl. Phys. Lett.* **1986**, *49*, 85.
[11] J. A. Nichols, H. W. H. Chan, M. A. B. Baker, *Biophys Rev.* **2019**, *11*111.
[12] M. Rupp, A. Tkatchenko, K. R. Müller, O. A. Lilienfeld, *Phys. Rev. Lett.* **2012**, *108*, 058301.
[13] J. G. Greener, S. M. Kandathil, L. Moffat, D. T. Jones, *Nat. Rev. Mol. Cell Biol.* **2022**, *23*, 40.
[14] M. S. Nitol, D. E. Dickel, C. D. Barrett, *Acta Mater.* **2022**, *224*, 117347.
[15] H. Zhu, W. Yan, Y. Liu, D. Hu, Y. Tu, Z. Huang, X. Tan, *Mater. Sci. Semicond. Process.* **2022**, *137*, 106198.
[16] X. Ding, M. Tao, J. Li, M. Li, M. Shi, J. Chen, Z. Tang, F. Benistant, J. Liu, *Mater. Sci. Semicond. Processing* **2022**, *143*, 106513.
[17] D. Liang, D. A. Frederick, E. E. Lledo, N. Rosenfield, V. Berardi, E. Linstead, U. Maoz, *Body Image* **2022**, *41*, 32.
[18] Z. Said, P. Sharma, A. K. Tiwari, V. V. Le, Z. Huang, V. G. Bui, A. T. Hoang, *J. Cleaner Prod.* **2022**, *360*, 132194.
[19] F. Camastra, V. Capone, A. Ciaramella, A. Riccio, A. Staiano, *Environ. Modell. Software* **2022**, *150*, 105343.
[20] Y. Torun, H. Doğan, *Superlattices Microstruct.* **2021**, *160*, 107062.
[21] T. Güzel, A. B. Çolak, *Superlattice Microstruct.* **2021**, *153*, 106864.
[22] A. B. Çolak, T. Güzel, O. Yıldız, M. Özer, *Phys. B Condens. Matter* **2021**, *608*, 412852.
[23] T. Güzel, A. B. Çolak, *Mater. Today Commun.* **2022**, *33*, 104175.
[24] O. Y. Olikh, *J. Appl. Phys.* **2015**, *118*, 024502.
[25] Y. Chang, W. Mao, Y. Hao, *Chinese J. Electron.* **2019**, *28*, 497.
[26] N. Karaboga, S. Kockanat, H. Dogan, *Appl. Intell.* **2013**, *38*, 279.
[27] T. Güzel, A. B. Çolak, *Phys. Status Solidi A* **2022**, *219*, 2100821.
[28] A. Rabehi, B. Nail, H. Helal, A. Douara, A. Ziane, M. Amrani, B. Akkal, Z. Benamara, *Superlattices Microstruct.* **2020**, *146*, 106665.
[29] B. Arıkan, S. Koçkanat, *Eur. J. Sci. Technol.* **2022**, *33*, 223.
[30] L. L. Li, J. L. Lou, M. L. Tseng, M. K. Lim, R. R. Tan, *Expert Syst. Appl.* **2022**, *203*, 117411.
[31] G. Tamilmani, V. B. Devi, T. Sujithra, F. H. Shajin, P. Rajesh, *Biomed. Signal Process. Control* **2022**, *75*, 103545.
[32] I. K. Gupta, A. Choubey, S. Choubey, *Comput. Electr. Eng.* **2022**, *102*, 108176.
[33] H. A. El-Sattar, S. Kamel, H. M. Sultan, H. M. Zawbaa, F. Jurado, *Energy Rep.* **2022**, *8*, 9506.
[34] H. Doğan, S. Duman, Y. Torun, S. Akkoyun, S. Dogan, U. Atıcı, *Mater. Sci. Semicond. Process.* **2022**, *149*, 106854.
[35] F. Zhang, L. J. O'Donnell, *Machine Learning: Methods and Applications to Brain Disorders*, Elsevier, Amsterdam **2019**, pp. 123–140, https://doi.org/10.1016/B978-0-12-815739-8.00007-9.
[36] C. Cortes, V. Vapnik, *Mach. Learn.* **1995**, *20*, 273.
[37] C. E. Rasmussen, H. Nickisch, *J. Mach. Learn. Res.* **2010**, *11*, 3011.
[38] J.-S. R. Jang, *IEEE Trans. Syst. Man. Cybern.* **1993**, *23*, 665.
[39] M. Sugeno, K. Tanaka, *Fuzzy Set Syst.* **1991**, *42*, 315.
[40] K. Wang, M. Ye, *Solid-State Electron.* **2009**, *53*, 234.
[41] K. Zervoudakis, S. Tsafarakis, *Comput. Ind. Eng.* **2020**, *145*, 106559.

© 2023 Wiley-VCH GmbH

18626319, 2023, 6, Downloaded from https://onlinelibrary.wiley.com/doi/10.1002/pssa.202200740 by Cumhuriyet University, Wiley Online Library on [10/01/2024]. See the Terms and Conditions (https://onlinelibrary.wiley.com/terms-and-conditions) on Wiley Online Library for rules of use; OA articles are governed by the applicable Creative Commons License